Ablative Rayleigh–Taylor instability in the limit of an infinitely large density ratio

Paul Clavin [*], Christophe Almarcha

*Institut de recherche sur les phénomènes hors équilibre, UMR 6594, CNRS-universités d'Aix-Marseille I & II,
49, rue Joliot-Curie, BP 146, technopôle de château-Gombert, 13384 Marseille cedex 13, France*

Presented by Paul Clavin

Abstract

The instability of ablation fronts strongly accelerated toward the dense medium under the conditions of inertial confinement fusion (ICF) is addressed in the limit of an infinitely large density ratio. The analysis serves to demonstrate that the flow is irrotational to first order, reducing the nonlinear analysis to solve a two-potential flows problem. Vorticity appears at the following orders in the perturbation analysis. This result simplifies greatly the analysis. The possibility for using boundary integral methods opens new perspectives in the nonlinear theory of the ablative RT instability in ICF. A few examples are given at the end of the Note. ***To cite this article: P. Clavin, C. Almarcha, C. R. Mecanique 333 (2005).***
© 2005 Académie des sciences. Published by Elsevier SAS. All rights reserved.

Résumé

Instabilité de Rayleigh–Taylor d'un front d'ablation dans la limite d'un rapport de densité infini. Dans les conditions de la fusion par confinement inertiel (FCI), on montre que l'écoulement associé à un front d'ablation fortement accéléré en direction du milieu dense est potentiel à l'ordre dominant de la limite infini du rapport de densité. La vorticité apparaît à l'ordre suivant de l'analyse en perturbation et l'étude non linéaire se réduit à celle d'un problème à deux potentiels de vitesse. Ce résultat simplifie grandement l'analyse et met l'étude des instabilités hydrodynamiques du front d'ablation en FCI sur de nouvelles bases en permettant l'utilisation de méthodes intégrales de frontières. Quelques exemples sont données à la fin de cette Note. ***Pour citer cet article : P. Clavin, C. Almarcha, C. R. Mecanique 333 (2005).***
© 2005 Académie des sciences. Published by Elsevier SAS. All rights reserved.

[*] Corresponding author.
  E-mail address: Clavin@irphe.univ-mrs.fr (P. Clavin).

Version française abrégée

L'objectif du confinement inertiel en fusion nucléaire (FCI) est d'atteindre au centre de l'implosion d'une capsule sphérique creuse de deuterium-tritium cryogénique remplie d'un mélange gazeux (rayon ≈ 2 mm, épaisseur $\approx 0{,}4$ mm) les conditions extrêmes de densité (≈ 300 g/cm^3) et température ($\approx 10^8$ K), voisines de celles à l'intérieur des étoiles, et qui sont nécessaires à l'initiation des réactions thermonucléaires [1]. En attaque directe, la capsule est soumise pendant une dizaine de nanosecondes à un intense rayonnement laser (10^{15} W/cm^2) qui, en ablatant sa face externe, produit une violente augmentation de pression (≈ 100 MBar) et provoque l'implosion. Dans les conditions envisagées pour un usage civil, les instabilités hydrodynamiques du front d'ablation fortement accéléré ($\approx 10^{11}$ m/s^2) sont susceptibles de compromettre la formation du point chaud et donc l'initiation des réactions nucléaires [1]. Ces instabilités font l'objet depuis plus d'une trentaine d'années d'intenses recherches théoriques et numériques. La théorie linéaire est maintenant à peu près bien comprise [2] et les études récentes s'orientent vers l'aspect non linéaire [3,4], dans le but de déterminer la géométrie de l'interface juste avant l'allumage. Les expériences étant lourdes et peu nombreuses [1,5], le phénomène complet est simulé par de puissants codes numériques développés au Lawrence Livermore Laboratory et au CEA/DIF. En parallèle, l'instabilité de Rayleigh–Taylor en présence de l'ablation est étudiée systématiquement sur des modèles simplifiés [2–4]. Nous présentons dans cette Note une nouvelle étape de ce développement. Sans ablation ni tension de surface, l'interface entre un fluide non visqueux et le vide (nombre d'Atwood unité, $A = 1$), soumise à l'instabilité de Rayleigh–Taylor (RT), prend la forme de bulles ascendantes et de d'aiguilles descendantes. Pour une solution périodique, la vitesse de la bulle tend vers une constante voisine de $\sqrt{g/3k}$ où g et k sont respectivement l'accélération et le nombre d'onde, alors que l'accélération de l'aiguille tend vers g. La formulation de ce problème est simple, l'écoulement est potentiel et la condition de pression sur l'interface facilement applicable grâce au théorème de Bernoulli. Son étude analytique et numérique vient de faire l'objet de progrès récents [6,7] qui déterminent l'évolution asymptotique du rayon de courbure à la pointe de l'aiguille ainsi que la manière dont son accélération approche g. Ces résultats reposent sur le caractère potentiel de l'écoulement qui se prête à l'utilisation de méthodes intégrales de frontières. En FCI le rapport de densité est très grand. Nous montrons dans cette Note que le problème avec ablation se simplifie grandement dans la limite d'un rapport de densité tendant vers l'infini, pour pouvoir être traité par les mêmes méthodes intégrales de frontières que celles utilisées pour l'instabilité de RT avec $A = 1$ [6,7]. Le modèle de départ a été développé précédemment [2,4], il est constitué d'un front d'ablation d'épaisseur négligeable soumis à un flux thermique fixé à l'infini aval et fortement accéléré dans la direction de ce flux. La vitesse de propagation du front plan dans le milieu dense $\bar{u}_-$ est nettement subsonique et l'écoulement au voisinage du front d'ablation est à faible nombre de Mach. Le front est assimilé à une isotherme et les effets hydrodynamiques sont décrits en supposant la densité constante de part et d'autre du front dans les équations d'Euler, $\rho_+ \ll \rho_-$. Les conditions de sauts appliquées sur le front traduisent la conservation de la masse, de l'impulsion et de l'énergie. La pertinence du modèle pour la FCI repose sur les trois points suivants : (i) l'absorption de l'énergie laser s'effectue à très haute température (faible densité fixée par l'égalité de la fréquence plasma et de celle du faisceau laser), et donc loin du front d'ablation ; (ii) la dépendance en température de la conductivité thermique de Spitzer $\lambda \propto T^{5/2}$ conduit à une séparation d'échelles ; lorsque la variation de température est grande, l'essentiel du saut de densité $(\rho_- - \rho)/\rho_- \approx 1$ se produit sur une distance petite devant l'épaisseur totale de l'onde thermique, $d_- \ll d_+$, voir Fig 1 ; (iii). Pour des nombres de Froude d'ordre unité rencontrés en FCI, $\bar{u}_-^2/g d_- = O(1)$, l'effet stabilisant de l'ablation aux petites échelles introduit une longueur d'onde marginale $\Lambda_m = \rho_- \bar{u}_-^2/\rho_+ g$ dont l'ordre de grandeur est intermédiaire, $d_- \ll \Lambda_m \ll d_+$ [2–4]. Dans ces conditions, une simplification importante apparaît : le problème thermique qui contrôle le flux de chaleur sur le front plissé, et donc la modification du taux d'ablation, se réduit à résoudre une équation de Laplace [2–4]. Ce point est délicat mais essentiel pour la suite. Une justification du modèle ainsi qu'une démonstration de l'équation proposée par Sanz et al. [3] sont données au paragraphe 2. La difficulté majeure qui subsiste dans l'étude du régime non linéaire provient de la création de vorticité à la traversée du front d'ablation. Nous montrons dans cette Note que, dans la limite $\rho_-/\rho_+ \to \infty (\varepsilon \equiv \rho_+/\rho_- \to 0)$, la partie rotationnelle de l'écoulement est d'ordre inférieur à la partie potentielle. L'ordre dominant de l'écoulement aval est

potentiel, comme l'écoulement amont. En effet, dans la limite $\varepsilon \to 0$, la vitesse de l'écoulement des produits ablatés est normale au front, et, le front étant une surface isotherme, on démontre que, comme pour le cas plan, l'ordre dominant de l'écoulement ablaté se déduit directement de la solution du problème thermique. Le problème non linéaire complet se met alors sous une forme faisant intervenir deux potentiels, l'un dans le fluide dense, l'autre dans les produits ablatés, reliés par un saut de pression sur le front obtenue aisément en utilisant l'équation de Bernoulli. Le problème se prête alors à un traitement numérique par la méthode intégrales de frontières utilisée récemment avec succès pour l'instabilité de Rayleigh–Taylor dans le cas d'un nombre d'Atwood unité [6,7] (Figs. 2 et 3). On démontre que, contrairement à la morphologie de la partie descendante, la vitesse de la bulle n'est pas modifiée par l'ablation. Quelques résultats numériques sont présentés, l'étude numérique systématique faisant l'objet d'une autre publication [8].

1. Introduction

A major challenge facing inertial confinement fusion is how to control the instability of the imploding capsule [1]. Large efforts have been undertaken over the three last decades to study the ablative Rayleigh–Taylor (RT) instability. The linear theory is now well developed [2], but the nonlinear growth of bubbles and spikes is still under investigation [3,4]. As in flame theory, a major difficulty in studying the nonlinear growth comes from the vorticity generated in the flow when crossing the ablation front. On the other hand, advances have been recently made in the long time evolution of the pure RT instability (inviscid, incompressible fluid without surface tension, bounded by a vacuum), thanks to boundary integral methods for potential flow models [6,7]. In this Note, we show that the ablative RT instability simplifies drastically in the limit of an infinitely large density ratio which is an accurate approximation in ICF. To first order, the nonlinear analysis reduces to solve two potential flows. The rotational part of the downstream flow may be taken into account at the second order in the perturbation analysis. Numerical results of ablative RT instabilities in ICF may then be obtained by boundary integral methods. We limit the presentation in this Note to a few examples of periodic solutions in two dimensional geometry compared with the pure RT instability. Detailed numerical analysis will be published elsewhere [8].

2. The model

The model is the same as in references [2] and [4]. The ablation front is an isotherm of the downstream flow, $\theta_+(\underline{r}, t) = \theta_f \gg 1$ where $\theta \equiv T/T_-$ is the nondimensional temperature reduced by its upstream value T_-. The temperature is uniform on the cold side $\theta_- = 1$, and the ablation front corresponds to a temperature jump, $\theta_f \gg 1$. Density is set constant in the Euler equations on both sides of the ablation front, $\rho_+ \ll \rho_-$. The relevance of such a piecewise constant density in the presence of a thermal gradient is discussed in this section. An intuitive explanation rests on the fact that most of the density variation $((\rho_- - \rho)/\rho_- \approx 1)$ is concentrated on the cold side across a thin region of extension d_- which is small compared with the total thickness of the thermal wave $d_- \ll d_+$, d_+ denoting the distance between the ablation front and the critical surface where the laser energy is absorbed, see Fig. 1. This is due to a large temperature variation across the thermal wave together with a temperature dependence of the heat conductivity in the form $\lambda \propto \theta^\nu$ with $\nu > 1$. The incompressible flow satisfies the Euler equations,

$$\rho_\pm D\underline{u}_\pm/Dt = -\underline{\nabla}(p_\pm + \rho_\pm gx), \qquad \underline{\nabla} \cdot \underline{u}_\pm = 0 \tag{1a}$$

with the following boundary conditions at infinity,

$$x \to -\infty: \lim_{x \to -\infty} \underline{u}_- \to \bar{u}_-\underline{i}, \quad \text{and} \quad x \to +\infty: \text{boundedness condition} \tag{1b}$$

where $\underline{i}$ is the unitary vector of the x-axis, $\bar{u}_-$ the absolute value of mean velocity of the ablation front relative to the cold medium, $\underline{u}_-(\underline{r}, t)$ and $\underline{u}_+(\underline{r}, t)$ are the upstream (dense and cold) and downstream (light and hot) flow
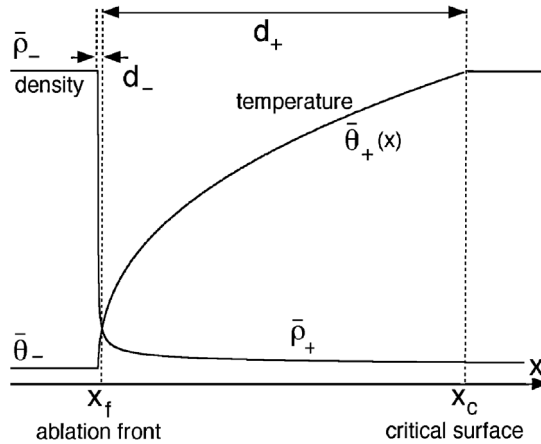
Fig. 1. Sketch of temperature and density profiles along the distance *x* across the unperturbed planar wave.

Fig. 1. Profils de température et de densité au sein de l'onde plane non perturbée.

velocities in the reference frame of the unperturbed wave, p denotes the pressure and g the acceleration. We assume a low Mach number approximation. The jump conditions across the ablation front refer to conservation of mass, momentum and energy. Conservation of mass yields

$$\rho_-(\underline{u}_- \cdot \underline{n} - u_n^{(f)})_{\underline{r}=\underline{r}_f} = \rho_+(\underline{u}_+ \cdot \underline{n} - u_n^{(f)})_{\underline{r}=\underline{r}_f} \equiv m \tag{2a}$$

where $\underline{r}_f$ is the position of the front, $\underline{n}$ the unitary vector (oriented toward the hot side) normal to the front, and $u_n^{(f)}$ is the normal velocity of the front in the reference frame of the unperturbed wave. Conservation of longitudinal and transverse momentum gives

$$\frac{p_-|_{\underline{r}=\underline{r}_f} - p_+|_{\underline{r}=\underline{r}_f}}{\rho_- \bar{u}_-^2} = \left(\frac{\rho_-}{\rho_+} - 1\right)\frac{m^2}{\rho_-^2 \bar{u}_-^2} \tag{2b}$$

$$\underline{u}_- \cdot \underline{t} = \underline{u}_+ \cdot \underline{t} \tag{2c}$$

where $\underline{t}$ is any tangent vector to the front. Conservation of energy at low Mach number gives

$$(\theta_f - 1)m/\rho_- \bar{u}_- = l_f \theta_f^\nu \underline{n} \cdot \underline{\nabla}\theta_+|_{\underline{r}=\underline{r}_f} \tag{2d}$$

where $l_f \equiv \lambda_-/C_p\rho_-\bar{u}_-$ is a reference length of the same order of magnitude as d_-. In the thick layer delimited by the ablation front and the critical surface the equation for the temperature $\theta_+(\underline{r}, t)$ is obtained from the energy conservation,

$$\partial(\rho_+\theta_+)/\partial t + \underline{\nabla} \cdot [\rho_+\underline{u}_+\theta_+ - \rho_-\bar{u}_- l_f \theta_+^\nu \underline{\nabla}\theta_+] = 0 \tag{3}$$

Eq. (2d) results from a spatial integration of Eq. (3) across the thin ablation front.

A constant density approximation in Eq. (3) is not compatible with a quasi-isobaric approximation. The validity of the piecewise constant density model is tricky. The model consists in neglecting the flow velocity disturbances induced by the density gradient in the hot region (downstream the ablation front) in front of those triggered by the deflection of the stream lines across the ablation front. Their ratio is of order $\Lambda_m/d_+ \ll 1$ as explained in [4]. This leads to neglecting the density variation in the Euler equations (1a) but not in the energy equation (3). Under a quasi-isobaric approximation, $\rho_+\theta_+ = \rho_-$ (Low Mach number and perfect gas law), Eq. (3) leads to the same law as proposed by Sanz et al. [3]

$$\Delta\theta_+^\nu = 0 \tag{4a}$$

as discussed now. Energy equation (3) subject to the quasi-isobaric approximation is written as $\underline{\nabla} \cdot [\rho_+ \underline{u}_+ \theta_+ - \rho_- \bar{u}_- l_f \theta_+^\nu \underline{\nabla} \theta_+] = 0$. Considering periodic solution in the transverse direction and a volume delimited by the ablation front s_f and any downstream isotherm surface s_+ located upstream to the critical surface, Eq. (3) leads to

$$\theta_+ \iint\limits_{s_+} [\rho_+ \underline{u}_+ - \rho_- \bar{u}_- l_f \theta_+^{\nu-1} \underline{\nabla} \theta_+] \cdot \underline{n} \, \mathrm{d}^2 s = \iint\limits_{s_f} \left[\theta_f \rho_+ \underline{u}_+ \cdot \underline{n} - (\theta_f - 1)m \right] \mathrm{d}^2 s$$

where (2d) has been used. Anticipating that the front velocity is smaller than the downstream flow velocity $u_n^{(f)}/\underline{u}_+ \cdot \underline{n} \ll 1$, approximation valid when $\rho_+/\rho_- \ll 1$ see Eq. (12c), one has, according to Eq. (2a), $m \approx \rho_+ \underline{n} \cdot \underline{u}_+|_{\underline{r}=\underline{r}_f}$, so that

$$\theta_+ \iint\limits_{s_+} [\rho_+ \underline{u}_+ - \rho_- \bar{u}_- l_f \theta_+^{\nu-1} \underline{\nabla} \theta_+] \cdot \underline{n} \, \mathrm{d}^2 s \approx \iint\limits_{s_f} \rho_+ \underline{u}_+ \cdot \underline{n} \, \mathrm{d}^2 s$$

For large temperature, $\theta_+ = \rho_-/\rho_+ \gg 1$, the term in the right-hand side is negligible in front of the first term in the left-hand side. The approximation $\iint_{s_+} \rho_- \bar{u}_- l_f (\theta_+^{\nu-1} \underline{\nabla} \theta_+) \cdot \underline{n} \mathrm{d}^2 s \approx \iint_{s_+} \rho_+ \underline{u}_+ \cdot \underline{n} \mathrm{d}^2 s$ is then valid along any isotherm at first order in the limit $\rho_+/\rho_- \to 0$. This leads to Eq. (4a) when $\underline{\nabla} \cdot (\rho_+ \underline{u}_+) \approx 0$. The validity of such a quasi-steady state approximation for the density in the hot region $\partial \rho_+/\partial \tau \approx 0$ is explained now. Ablation stabilizes perturbations of short wavelengths and the marginal wavelength $\Lambda_m = 2\pi \rho_- \bar{u}_-^2/\rho_+ g$ lies in an intermediate range, $d_- \ll \Lambda_m \ll d_+$ when the Froude number is of order unity, $F_r^{-1} \equiv g l_f/\bar{u}_-^2 = \mathrm{O}(1)$, see Section 3. For such wrinkles, the relaxation time by transverse heat diffusion in the hot region is faster than the evolution time of the ablation front controlled by convection–diffusion balance, $\partial/\partial t \ll \underline{u}_+ \cdot \underline{\nabla} \approx \bar{u}_+ l_f \underline{\nabla} \cdot (\theta_+^\nu \underline{\nabla})$. Temperature and density in the hot region then reach a quasi-steady state approximation. To summarize, Eq. (4a) is valid under conditions $\theta_+ \gg 1 (\rho_+/\rho_- \to 0)$ and $\underline{\nabla} \cdot (\rho_+ \underline{u}_+) \approx 0$. Notice also that Eq. (4a) is compatible with the steady planar solution of Eq. (3) $\rho_+ \underline{u}_+ = \rho_- \bar{u}_- \underline{i}$, $(\theta_+ - 1) - l_f \theta_+^\nu \mathrm{d}\theta_+/\mathrm{d}x = 0$, $\Rightarrow \mathrm{d}^2 \theta_+^\nu/\mathrm{d}x^2 \approx 0$ for $\theta_+ \gg 1$.

The temperature disturbances generated by the wrinkles of the ablation front die out exponentially quickly over a distance of order Λ toward the hot side. The critical surface is not perturbed in the first approximation for $\Lambda \ll d_+$, [2–4]. In the reference frame moving with the mean position of the ablation front, the boundary condition at infinity to be used with Eq. (4a) is

$$x \to +\infty: \theta_+^\nu(\underline{r}, t) \to \bar{\theta}^\nu(x) \tag{4b}$$

where $\bar{\theta}^\nu(x)$ is the steady state solution (unperturbed planar wave) which may be written as

$$x \geqslant \bar{x}_f: \bar{\theta}^\nu(x) \equiv \nu(x - \bar{x}_f)(1 - 1/\theta_f) + \theta_f^\nu \tag{4c}$$

valid up to the first order in a powers expansion in $1/\theta_f$ for $\theta_f \gg 1$ and $0 \leqslant (x - \bar{x}_f)\nu \ll \theta_f^\nu$. Introducing $\Psi'(\underline{r}, t) \equiv [\theta_+^\nu(\underline{r}, t) - \bar{\theta}^\nu(x)]/(1 - \theta_f^{-1})\nu$, one obtains, according to (4a–c),

$$\Delta \Psi' = 0 \quad \text{with } \Psi'(\underline{r} = \underline{r}_f, t) = -\left[x_f(t) - \bar{x}_f \right] \quad \text{and} \quad x \to +\infty: \Psi' = 0 \tag{4d}$$

3. Nondimensional equations

From now on we will use nondimensional variables,

$$\underline{u}_\pm/\bar{u}_- \to \underline{u}_\pm, \quad (p_\pm + \rho_\pm g x)/\rho_- \bar{u}_-^2 \to \pi_\pm, \quad m/\rho_- \bar{u}_- \to \mu, \quad \underline{r}/l_f \to \underline{r}, \quad t\bar{u}_-/l_f \to t \tag{5}$$

The model defined by Eqs. (1a,b) (2a–d) and (4a–) introduces two parameters $F_r^{-1} \equiv g l_f/\bar{u}_-^2$ and $\varepsilon \equiv \rho_+/\rho_-$. Within the quasi-isobaric approximation the reduced temperature at the front is $\theta_f = 1/\varepsilon$. After introducing the splitting $a = \bar{a} + a'$ where $\bar{a}$ represents the steady planar solution, Eqs. (1a,b), (4d) and (2a–d) can be written in nondimensional form as,

$$\frac{\partial \underline{u}'_-}{\partial t} + \frac{\partial \underline{u}'_-}{\partial x} + (\underline{u}'_- \cdot \underline{\nabla})\underline{u}'_- = -\underline{\nabla}\pi'_-, \quad \varepsilon\frac{\partial \underline{u}'_+}{\partial t} + \frac{\partial \underline{u}'_+}{\partial x} + \varepsilon(\underline{u}'_+ \cdot \underline{\nabla})\underline{u}'_+ = -\underline{\nabla}\pi'_+, \quad \underline{\nabla} \cdot \underline{u}'_\pm = 0 \tag{6a}$$

with

$$x \to -\infty: \underline{u}'_- \to 0 \quad \text{and} \quad x \to +\infty: \text{boundedness condition} \tag{6b}$$

$$\Delta \Psi' = 0 \quad \text{with} \quad x \to +\infty: \Psi' = 0 \tag{6c}$$

$$\underline{r} = \underline{r}_f : \left(\underline{u}'_- \cdot \underline{n} - u_n'^{(f)}\right) = \varepsilon\left(\underline{u}'_+ \cdot \underline{n} - u_n'^{(f)}\right) \equiv (1 - \underline{i} \cdot \underline{n}) + \mu', \bar{\mu} = 1 \tag{7a}$$

$$\underline{u}_- \cdot \underline{t} = \underline{u}_+ \cdot \underline{t} \Rightarrow (\underline{u}'_- \cdot \underline{t} - \underline{u}'_+ \cdot \underline{t}) = (1 - \varepsilon)\underline{i} \cdot \underline{t}/\varepsilon \tag{7b}$$

$$\pi_- - \pi_+ = (1 - \varepsilon)(1 + \mu')^2/\varepsilon - F_r^{-1}(1 - \varepsilon)x_f \tag{7c}$$

$$\Psi' = -(x_f - \bar{x}_f), \quad \text{and} \quad 1 + \mu' = \underline{n} \cdot (\underline{i} + \underline{\nabla}\Psi') \tag{7d}$$

the last equation (7d) is the nondimensional form of Eq. (2d).

4. Ordering and scaling laws in the limit $\varepsilon \to 0$

The linear stability analysis provides us with the ordering in the limit $\varepsilon \to 0$ [4]. Considering 2D perturbations for simplicity and choosing the origin of the x-axis at the unperturbed front, the equation of the perturbed ablation front is expressed as $x = x_f(y, t)$. Using a normal modes decomposition $x_f = \tilde{x}_f(k)\,\mathrm{e}^{\mathrm{i}\underline{k}\cdot\underline{y}+\sigma t}$ with $k \equiv |\underline{k}|$, any perturbed field can be written as $a'(x, y, t) = \tilde{a}(x, k)\tilde{x}_f(k)\,\mathrm{e}^{\mathrm{i}\underline{k}\cdot\underline{y}+\sigma t}$, $\mu' = \tilde{\mu}(k)\tilde{x}_f(k)\,\mathrm{e}^{\mathrm{i}\underline{k}\cdot\underline{y}+\sigma t}$. The solution of the linearized equations (6a–b) can be expressed in terms of three constants of integration $\widetilde{U}_-$, $\widetilde{U}_{p+}$ and $\widetilde{U}_{r+}$ as,

$$\tilde{u}_- = \widetilde{U}_-\,\mathrm{e}^{kx}, \qquad \tilde{\pi}_- = -\frac{\sigma + k}{k}\widetilde{U}_-\,\mathrm{e}^{kx} \tag{8a}$$

$$\tilde{u}_+ = \widetilde{U}_{p+}\,\mathrm{e}^{-kx} + \widetilde{U}_{r+}\,\mathrm{e}^{-\varepsilon\sigma x}, \quad \tilde{\pi}_+ = \frac{\varepsilon\sigma - k}{k}\widetilde{U}_{p+}\mathrm{e}^{-kx}, \quad \mathrm{i}\underline{k} \cdot \underline{v}_\pm = -\partial u_\pm/\partial x \tag{8b}$$

where $\widetilde{U}_{p+}$ and $\widetilde{U}_{r+}$ represent respectively the potential and rotational part of the downstream flow. The solution of Eqs. (6c) and (7d) yields

$$\tilde{\mu}(k) = k \quad \text{where } k \equiv \sqrt{\underline{k} \cdot \underline{k}} \tag{9a}$$

The constants are obtained from Eqs. (7a–b),

$$\widetilde{U}_- = k + \sigma, \quad (k - \varepsilon\sigma)\widetilde{U}_{r+} = +2k(\sigma + k), \quad (k - \varepsilon\sigma)\widetilde{U}_{p+} = \frac{1 - \varepsilon}{\varepsilon}k^2 - 2k\sigma - (\varepsilon\sigma^2 + k^2) \tag{9b}$$

Finally, by using Eq. (9b) and substituting Eqs. (8a–b) and (9a) for $\pi_\pm$ and μ' into Eq. (7c), the following dispersion relation is obtained,

$$(1 + \varepsilon)\sigma^2 + 4k\sigma - \left[F_r^{-1}(1 - \varepsilon k) - \frac{1 + \varepsilon}{\varepsilon}k^2\right] = 0 \tag{10a}$$

For small ε, the reduced marginal wave number and the reduced maximal growth rate are of order εF_r^{-1} and $\varepsilon^{1/2}F_r^{-1}$ respectively. Introducing two quantities of order unity κ and s,

$$k \equiv \varepsilon F_r^{-1}\kappa, \quad \kappa = \mathrm{O}(1), \quad \sigma = \varepsilon^{1/2}F_r^{-1}s, \quad s = \mathrm{O}(1) \tag{10b}$$

the dispersion relation (10a) takes the simple form $s^2 - [\kappa - \kappa^2] = 0$ at the first approximation in the limit $\varepsilon \to 0$.

The order of magnitude of the nondimensional flow fields, expressed in terms of the nondimensional amplitude of the perturbed ablation front x_f, are obtained from (8a,b) and (9a,b),

$$\bar{\mu} = 1, \quad \mu'/x_f = \mathrm{O}\big(\varepsilon F_r^{-1}\big), \quad \underline{u}'_-/x_f = \mathrm{O}\big(\varepsilon^{1/2} F_r^{-1}\big), \quad \pi'_-/x_f = \mathrm{O}\big(F_r^{-1}\big) \tag{11a}$$

$$\underline{u}'_+/x_f = \mathrm{O}\big(F_r^{-1}\big), \qquad \pi'_+/x_f = \mathrm{O}\big(F_r^{-1}\big) \tag{11b}$$

Notice that, according to Eqs. (9b) and (10b), the rotational part of the downstream flow is smaller than the potential part by a factor $\varepsilon^{1/2}$. We show in the next section that this is also true in the nonlinear case.

5. Nonlinear theory in the limit $\varepsilon \to 0$

Considering length and time scales of the same order of magnitude as the most linearly amplified wavelength (and its linear growth time), the nondimensional coordinates useful for solving the nonlinear problem are, according to Eqs. (5) and (10b),

$$\underline{\xi} \equiv \big(\varepsilon F_r^{-1}\big)\underline{r}/l_f, \qquad \tau \equiv \big(\varepsilon^{1/2} F_r^{-1}\big)\bar{u}_- t/l_f \tag{12a}$$

In this system of coordinates, τ and $\underline{\xi} = (\xi, \underline{\eta})$ where ξ and $\underline{\eta}$ are the longitudinal and transverse coordinates, the coordinates of the ablation front will be denoted by $\underline{\xi}_f$, solution of the unknown equation of the front $f(\underline{\xi}_f, \tau) = 0$. Considering corrugations of the ablation front with amplitude of the same order of magnitude as the most linearly amplified wavelength, nondimensional quantities of order unity in the limit $\varepsilon \to 0$ are introduced from Eqs. (5), (11a,b) and (12a),

$$m/\rho_- \bar{u}_- = \mu(\underline{\xi}_f, \tau), \quad \underline{u}'_-/\bar{u}_- = \varepsilon^{-1/2} \underline{U}'_-(\underline{\xi}, \tau), \quad \pi'_- = \varepsilon^{-1} \Pi'_-(\underline{\xi}, \tau) \tag{12b}$$

$$u_n^{(f)}/\bar{u}_- = \varepsilon^{-1/2} U_n^{(f)}, \quad \underline{u}'_+/\bar{u}_- = \varepsilon^{-1} \underline{U}'_+(\underline{\xi}, \tau), \quad \pi'_+ = \varepsilon^{-1} \Pi'_+(\underline{\xi}, \tau) \tag{12c}$$

The Euler equations (1a) and (6a) yield

$$\left[\frac{\partial}{\partial \tau} + \varepsilon^{1/2}\frac{\partial}{\partial \xi}\right]\underline{U}'_- + (\underline{U}'_- \cdot \widetilde{\nabla})\underline{U}'_- = -\widetilde{\nabla}\Pi'_-, \qquad \widetilde{\nabla} \cdot \underline{U}'_- = 0 \tag{12d}$$

$$\left[\varepsilon^{1/2}\frac{\partial}{\partial \tau} + \frac{\partial}{\partial \xi}\right]\underline{U}'_+ + (\underline{U}'_+ \cdot \widetilde{\nabla})\underline{U}'_+ = -\widetilde{\nabla}\Pi'_+, \qquad \widetilde{\nabla} \cdot \underline{U}'_+ = 0 \tag{12e}$$

where $\widetilde{\nabla}$ denotes the spatial derivative with respect to $\underline{\xi} = (\xi, \underline{\eta})$. Eqs. (12d) express that the unperturbed flow is negligible upstream and the perturbed flow is quasi-steady downstream in the first approximation.

According to Eqs. (11a,b), the normal velocity of the perturbed front $u_n^{(f)}$ and the perturbations of the upstream flow velocity $\underline{u}'_-$ are larger than the ablation velocity $\bar{u}_-$ by a factor $\varepsilon^{-1/2}$, but smaller than the perturbations of the downstream flow velocity $\underline{u}'_+$ by a factor $\varepsilon^{1/2}$.

From now on, we will consider only the leading order term in the limit $\varepsilon \to 0$. According to Eqs. (7a) mass conservation across the ablation front leads to,

$$\underline{n} \cdot \underline{U}'_-|_{\underline{\xi}=\underline{\xi}_f} = U_n^f, \qquad \underline{n} \cdot (\underline{i} + \underline{U}'_+)|_{\underline{\xi}=\underline{\xi}_f} = 1 + \mu' \tag{13a}$$

The first equation is the same kinematics condition as in the RT problem; to first order, the ablation velocity is negligible in front of the upstream flow velocity. Together with the second equation (7d) (conservation of energy at the front) the last equation (13a) yields,

$$\underline{n} \cdot \underline{U}'_+|_{\underline{\xi}=\underline{\xi}_f} = \underline{n} \cdot \widetilde{\nabla}\Psi|_{\underline{\xi}=\underline{\xi}_f} \tag{13b}$$

where $\Psi = \varepsilon F_r^{-1}\Psi'$ so that $\underline{\nabla}\Psi'|_{\underline{r}=\underline{r}_f} = \widetilde{\nabla}\Psi|_{\underline{\xi}=\underline{\xi}_f}$.

On the other hand, according to the first equation (7d), $\underline{t} \cdot \widetilde{\nabla}\Psi|_{\underline{\xi}=\underline{\xi}_f} = -\underline{i} \cdot \underline{t}$, together with the second equation (7b), $\underline{t} \cdot \underline{U}'_+|_{\underline{\xi}=\underline{\xi}_f} = -\underline{i} \cdot \underline{t}$, one gets,

$$\underline{t} \cdot \underline{U}'_+|_{\underline{\xi}=\underline{\xi}_f} = \underline{t} \cdot \widetilde{\nabla}\Psi|_{\underline{\xi}=\underline{\xi}_f} \tag{13c}$$

Eqs. (13b–c) then show that the downstream flow is potential at the ablation front,

$$\underline{U}'_+|_{\underline{\xi}=\underline{\xi}_f} = \widetilde{\underline{\nabla}}\Psi|_{\underline{\xi}=\underline{\xi}_f} \tag{14a}$$

Since, according to the Euler equations (12e) for constant density, vorticity is simply convected downstream and cannot be created elsewhere than across the ablation front, Eq. (14a) shows that the downstream flow is potential,

$$\underline{U}'_+ = \widetilde{\underline{\nabla}}\Psi \tag{14b}$$

The flow is slaved by the thermal problem, in a way similar to the planar wave in the quasi-isobaric approximation. Without perturbations at $\xi = -\infty$, the upstream flow is also potential,

$$\underline{U}'_- = \widetilde{\underline{\nabla}}\Phi. \tag{14c}$$

The Euler equations (12d,e) may then be written in the simple form

$$\frac{\partial}{\partial\tau}\underline{U}'_- = -\widetilde{\underline{\nabla}}\big[\Pi'_- + |\underline{U}'_-|^2/2\big], \quad \widetilde{\underline{\nabla}}\cdot\underline{U}'_- = 0, \quad \frac{\partial}{\partial\xi}\underline{U}'_+ = -\widetilde{\underline{\nabla}}\big[\Pi'_+ + |\underline{U}'_+|^2/2\big], \quad \widetilde{\underline{\nabla}}\cdot\underline{U}'_+ = 0 \tag{15a}$$

leading to the following Bernoulli equations,

$$\Pi'_- = -\partial\Phi/\partial\tau - |\widetilde{\underline{\nabla}}\Phi|^2/2, \qquad \Pi'_+ = -\partial\Psi/\partial\xi - |\widetilde{\underline{\nabla}}\Psi|^2/2 \tag{15b}$$

where two functions of time have been omitted and are incorporated in the definition of the potentials Φ and Ψ. According to Eq. (7c), the leading order of the pressure jump may be written as,

$$[\Pi'_- - \Pi'_+]_{\underline{\xi}=\underline{\xi}_f} = (1+\mu')^2 - 1 - (\xi_f - \bar{\xi}_f) \tag{15c}$$

6. Final result

To first order, the nonlinear problem reduces to a free boundary problem, $f(\underline{\xi}_f, \tau) = 0$, consisting in solving two potential flows with a boundary condition (15c) at the front written, according to Eqs. (15b) and the second equation (13a), as

$$\left[-\frac{\partial\Phi}{\partial\tau} + \frac{\partial\Psi}{\partial\xi} - \frac{|\widetilde{\underline{\nabla}}\Phi|^2}{2} + \frac{|\widetilde{\underline{\nabla}}\Psi|^2}{2}\right]_{\underline{\xi}=\underline{\xi}_f} = \big[\underline{n}\cdot(\underline{i} + \widetilde{\underline{\nabla}}\Psi)|_{\underline{\xi}=\underline{\xi}_f}\big]^2 - 1 - (\underline{\xi}_f - \bar{\underline{\xi}}_f)\cdot\underline{i} \tag{16a}$$

where $\underline{i}$ is the unitary vector in the direction of the acceleration (opposite direction to the energy flux prescribed at downstream infinity). According to Eqs. (7) and (15a) the two velocity potentials are solutions of

$$\tilde{\Delta}\Psi = 0 \quad \text{with } \xi \to +\infty\colon \Psi = 0 \quad \text{and} \quad \Psi|_{\underline{\xi}=\underline{\xi}_f} = -(\underline{\xi}_f - \bar{\underline{\xi}}_f)\cdot\underline{i} \tag{16b}$$

$$\tilde{\Delta}\Phi = 0 \quad \text{with } \xi \to -\infty\colon \Phi = 0 \quad \text{and} \quad \underline{n}\cdot\widetilde{\underline{\nabla}}\Phi|_{\underline{\xi}=\underline{\xi}_f} = U_n^f \tag{16c}$$

where U_n^f is the normal velocity of the front. The last equation (16c) is a purely kinematical condition in which the ablation velocity is negligible in the limit $\varepsilon \to 0$.

When the equation of the front may be written in the form $\xi = \xi_f(\eta, \tau)$, the reduced normal velocity is defined as $U_n^{(f)} = (\partial\xi_f/\partial\tau)[1 + (\partial\xi_f/\partial\eta)^{-2}]^{-1/2}$, and the relation $\underline{n}\cdot(\underline{i} + \widetilde{\underline{\nabla}}\Psi)|_{\underline{\xi}=\underline{\xi}_f} = [1 + \partial\Psi/\partial\xi|_{\xi=\xi_f}][1 + (\partial\xi_f/\partial\eta)^2]^{1/2}$ is obtained by using the second equation (13c). The linear solution is then recovered from Eq. (16a), by using $\partial\xi_f/\partial\tau \approx \partial\Phi/\partial\xi|_{\xi=0}$ and $\underline{n}\cdot(\underline{i} + \widetilde{\underline{\nabla}}\Psi)|_{\xi=0} \approx 1 + \partial\Psi/\partial\xi|_{\xi=0}$.
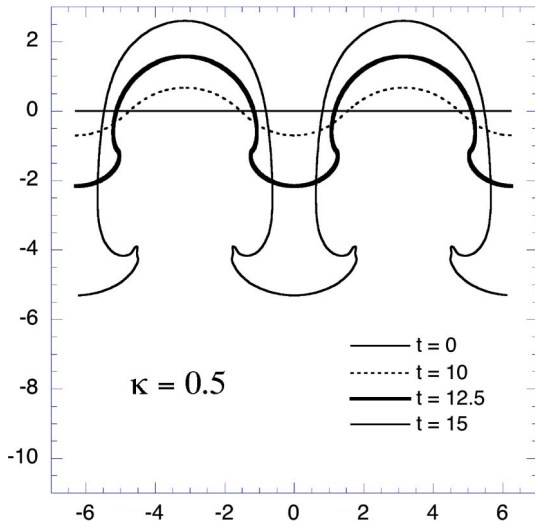
Fig. 2. Two-dimensional solutions of Eqs. (16) at various times. The initial condition is $\Phi(\xi, \eta, \tau = 0) = 0$ and a sine-mode for $\xi(\eta, \tau = 0)$ corresponding to the most linearly instable wave number $k = 0.5\varepsilon g/\bar{u}_-^2 (\kappa = 0.5)$ with amplitude $0.01/k$. At time $t = 12.5\varepsilon^{-1/2}\bar{u}_-/g (\tau = 12.5)$, a singularity of the slope appears at the inflexion point on the side of the spike.

Fig. 2. Évolution de la surface d'ablation au cours du temps à partir d'une perturbation initiale sinusoïdale dont la longueur d'onde est linéairement la plus instable $k = 0,5\varepsilon g/\bar{u}_-^2 (\kappa = 0,5)$ et dont l'amplitude vaut $0,01/k$. On observe une singularité de pente qui se développe au point d'inflexion sur le côté de l'aiguille au temps $t = 12,5\varepsilon^{-1/2}\bar{u}_-/g (\tau = 12,5)$.
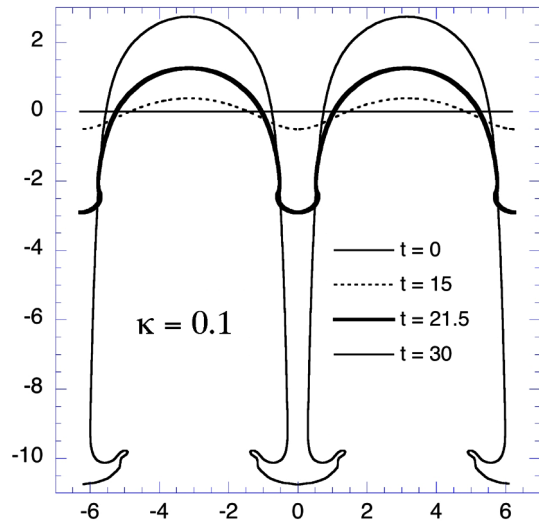
Fig. 3. Two-dimensional solutions of Eqs. (16) at various times. The initial condition is $\Phi(\xi, \eta, \tau = 0) = 0$ and a sine-mode for $\xi(\eta, \tau = 0)$ corresponding to the wave number $k = 0.1\varepsilon g/\bar{u}_-^2 (\kappa = 0.1)$ with amplitude $0.01/k$. At time $t = 21.5\varepsilon^{-1/2}\bar{u}_-/g_- (\tau = 21.5)$, a singularity of the slope appears at the inflexion point on the side of the spike.

Fig. 3. Évolution de la surface d'ablation au cours du temps à partir d'une perturbation initiale sinusoïdale dont la longueur d'onde est $k = 0,1\varepsilon g/\bar{u}_-^2 (\kappa = 0,1)$ et dont l'amplitude vaut $0,01/k$. On observe une singularité de pente qui se développe au point d'inflexion sur le côté de l'aiguille au temps $t = 21,5\varepsilon^{-1/2}\bar{u}_-/g_- (\tau = 21,5)$.

7. Discussion and perspectives

The only parameter left in Eqs. (16) is the size L of the box, or in nondimensional form, the inverse of a Froude number, $(\rho_+/\rho_-)gL/2\pi\bar{u}_-^2$, which measures the number of linearly unstable modes. We present below preliminary numerical results for two-dimensional periodic solutions of Eqs. (16) obtained thanks to the boundary integral method used recently for the Rayleigh–Taylor instability with a unity Atwood number [7]. The results concern two wave numbers $\kappa = 0.5$ (the most linearly amplified one with the reduced growth rate $s = 0.5$) in Fig. 2 and $\kappa = 0.1$ ($s = 0.3$) in Fig. 3. We start with a sine-mode whose amplitude equals wavelength/(200π). The formation of bubbles and spikes is exhibited soon after few characteristic linear growth times, typically six. After a time about $\tau = 15$ for $\kappa = 0.5$ and $\tau = 30$ for $\kappa = 0.1$, the bubble velocity reaches the same value as for the classical Rayleigh–Taylor instability with a unity Atwood number (without ablation). Using a Layzer-type approach [9], it may be easily shown directly from Eqs. (16) that the asymptotic velocity of the bubble is effectively $\sqrt{g/3k}$. A singularity in the slope appears in the numerical simulations at $\tau = 12.5$ for $\kappa = 0.5$ and $\tau = 21.7$ for $\kappa = 0.1$. The overall shape looks similar to the one obtained by Sanz et al. [3]. It is not yet clear that the following orders in the ε expansion and/or additional curvature terms could regularize the singularity. However, as shown in Figs. 2 and 3, the numerical simulations have been carried out beyond the occurrence of the singularity without much trouble by smoothing out the cusp. The tip of the spike is strongly affected by ablation. Its acceleration increases and seems to approach g after a time delay longer than in the Rayleigh–Taylor case. Except in the neighborhood of this tip, the shape of the front is similar to the solution of the classical Rayleigh–Taylor instability with a unity

Atwood number. The relevance of the model and of the numerical results for such large amplitude of the spike as in Figs. 2 and 3 is questionable. Further studies are under investigations to clarify the situation [8].

It is worth recalling that in real experiments in ICF the duration of implosion is typically 10 times the characteristic growth time of the most amplified wavelength. This corresponds here to $\tau \approx 20$. Concerning real experiments, reliable predictions require further investigations. There are two competitive geometrical effects that are not included in the present analysis; ablation consumes the spike while implosion amplifies the disturbances (Bell–Plesset effect). The first one may be taken into account by pushing the analysis to the following order, and the second one is not difficult to be included provided that the wavelength remains small compare to the radius, which is effectively the case. The present work will be extended to include these effects in the near future. Another problem to be addressed with our approach is the wavelength selection when starting with a distributed spectrum of initial disturbances.

Acknowledgements

References

[1] S. Atzeni, J. Meyer-Ter-Vehn, The Physics of Inertial Fusion, Clarendon Press, Oxford, 2004.
[2] L. Masse, Étude linéaire de l'instabilité du front d'ablation en fusion par confinement inertiel, Thèse de l'Université de Provence 23, novembre 2001.
[3] J. Sanz, J. Ramirez, R. Ramis, R. Betti, R.P.J. Town, Nonlinear theory of the ablative Rayleigh Taylor instability, Phys. Rev. Lett. 89 (19) (2002) 195002.
[4] P. Clavin, L. Masse, Instabilities of ablation fronts in inertial confinement fusion: a comparison with flames, Phys. Plasmas 11 (2) (2004) 690–705.
[5] B.A. Remington, S.W. Haan, S.G. Glendinning, J.D. Kilkenny, D.H. Munro, R.J. Wallace, Large growth Rayleigh–Taylor experiments used shaped laser pulses, Phys. Rev. Lett. 67 (1991) 3259–3262.
[6] P. Clavin, F. Williams, Asymptotic spike evolution in Rayleigh–Taylor instability, J. Fluid. Mech. 525 (2005) 105–113.
[7] L. Duchemin, C. Josserand, P. Clavin, Asymptotic behaviour of the Rayleigh–Taylor instability, Phys. Rev. Lett. (2005), submitted for publication.
[8] C. Almarcha, L. Duchemin, C. Josserand, P. Clavin, 2005, in preparation.
[9] D. Layzer, On the instability of superposed fluids in a gravitational field, Astrophys. J. 122 (1955) 1–12.